Catalysis Letters 25 (1994) 75–86



# Methane coupling at low temperatures on Ru(0001) and Ru(11$\bar{2}$0) catalysts

Petra Lenz-Solomun [1], Ming-Cheng Wu and D. Wayne Goodman [2]

*Department of Chemistry, Texas A&M University, College Station, TX 77843-3255, USA*

Received 18 June 1993; accepted 6 December 1993

The conversion of methane to higher hydrocarbons on single crystal Ru catalysts has been investigated using combined elevated-pressure kinetic measurements/surface science studies. The reaction consists of activation of methane on Ru(0001) and Ru(11$\bar{2}$0) surfaces to produce carbonaceous intermediates at temperatures ($T_{CH_4}$) between 350 and 700 K and rehydrogenation of these species to ethane and propane at $T_{H_2} \approx 370$ K. It is found that under the reaction conditions employed, the maximum yield in ethane/propane production occurs at $T_{CH_4} \approx 500$ K on both surfaces. Influence of the hydrogenation temperature on the production of ethane and propane is also examined. On Ru(0001), the yields of ethane and propane maximize at $T_{H_2} = 400$ K, whereas no maximum yield was observed on Ru(11$\bar{2}$0) in the 300–500 K temperature range. Under optimum reaction conditions, hydrocarbon products consist of 16% ethane and 2% propane. High-resolution electron energy-loss spectroscopy (HREELS) has been used to identify various forms of hydrocarbonaceous intermediates following methane decomposition. An effort is made to relate the hydrocarbon intermediates identified by HREELS to the gas phase products observed in the elevated pressure experiments.

**Keywords:** Methane conversion; single crystal Ru catalyst; kinetic studies; surface science studies

## 1. Introduction

The catalytic conversion of methane to higher hydrocarbons has become of great economic interest in the past decade. Methane activation is particularly challenging because of its unusual high stability. Strong tetrahedral C–H bonds of methane offer no polar distortions to facilitate chemical attack. A current practice in methane conversion utilizes an indirect route in which methane is first converted to a synthesis gas at high temperatures. Higher hydrocarbons are subsequently obtained via Fischer–Tropsch synthesis [1–3]. A promising approach for direct conversion is the oxidative coupling of methane over metal oxide catalysts [4–8], a reaction that proceeds at temperatures between 850 and 1200 K with hydrocarbon yield up to 25% [9]. In order to become economically more attractive, it is vital to

[1] Present address: Fritz-Haber-Institut der Max-Planck-Gesellschaft, Faraday 4-6, D-1000 Berlin 33, Germany.

[2] To whom correspondence should be addressed.

increase the overall selectivity to ethane and to improve the lifetime of catalysts. An alternative, two-step approach, suggested by van Santen and co-workers [10–12], consists of activation of methane on supported transition metal catalysts to produce carbonaceous intermediates between 350 and 850 K and rehydrogenation of these species to higher hydrocarbons at ~ 370 K.

Due to a positive change of the Gibbs free energy, the direct conversion of methane to ethane is not thermodynamically allowed. This limitation may be circumvented by introducing oxidants, such as $O_2$ and $Cl_2$, during reaction. The presence of the oxidants effectively decreases the Gibbs free energy, but also provides a more favorable path for methane combustion. An alternative solution is to divide the overall reaction into two steps. In the first step, the accompanying change in entropy is negative, whereas the enthalpy change is positive. Therefore, methane decomposition is carried out at high temperatures. The second-step reaction involves rehydrogenation of carbonaceous deposits to form higher hydrocarbons. This reaction is exothermic and occurs only at relatively low temperatures.

Methane decomposition on transition metal surfaces is an activated process with activation energies ranging from 25 to 60 kJ/mol [13–20]. These energies are lower than those for CO decomposition; however, methane decomposition is carried out at higher temperatures. The principal reason for this contrast is due to the extremely low sticking probability of methane. Methane activation has been suggested to proceed via a proton tunneling mechanism, and it is believed that the initial proton tunneling determines methane decomposition rates [20,21]. Ceyer and co-workers [22–25] have demonstrated, with the use of molecular beam techniques, the importance of translational energies in methane decomposition on a Ni(111) surface.

Various forms of surface carbonaceous species from methane decomposition on silica supported Ru, Rh and Co catalysts have been investigated by van Santen and co-workers [10–12]. Three forms of surface carbon species are distinguishable from their ability to form methane during hydrogenation. By analogy to carbonaceous deposits identified by Bell and co-workers in studies of CO hydrogenation [26–28], these species were designated as $C_\alpha$, $C_\beta$ and $C_\gamma$ species and suggested to correspond to carbidic, amorphous and graphitic carbon, respectively [10–12].

In this article, we report the results of combined elevated-pressure kinetic measurements/surface science studies of the ethane and propane formation from methane over Ru catalysts using the two-step approach. The focus of this article is to address the kinetics of ethane and propane formation. An effort is also made to relate surface hydrocarbonaceous intermediates identified with surface science techniques to gas phase products observed in the elevated pressure experiments.

## 2. Experimental

The studies were carried out in two ultrahigh vacuum (UHV) systems. The kinetic data were acquired in a combined elevated-pressure reactor/UHV surface

analysis chamber equipped with Auger electron spectroscopy (AES) and temperature programmed desorption (TPD). A separate UHV system containing high resolution electron energy loss spectroscopy (HREELS) and a micoreactor was employed to characterize various forms of surface hydrocarbon species following methane decomposition. This second UHV system also has capabilities for AES, low energy electron diffraction (LEED) and TPD, and for sample heating and cooling. The details of this UHV system have been described elsewhere [29].

The Ru(0001) and Ru(11$\bar{2}$0) specimens were chosen as the catalysts with separate experiments run for each sample. Crystal temperatures were monitored with a W/5%Re–W/26%Re thermocouple spot-welded to the back of the crystal. The crystal cleaning procedure consisted of mild argon ion sputtering, heating in $4 \times 10^{-7}$ Torr $O_2$ at 1100 K, and annealing to 1400–1500 K. Surface cleanliness was verified by using the peak-to-peak height ratio of the Ru(273 eV) to Ru(231 eV) Auger signals [30]. The details of crystal cleaning and handling can be found elsewhere [31,32].

Methane and hydrogen gases were purchased from Matheson at a nominal purity of 99.996% and 99.9995%, respectively. Methane gas was purified using the following procedure: (1) $CH_4$ gas from the stainless steel cylindrical bottle was condensed into a zeolite trap cooled with liquid nitrogen; (2) the gas was subsequently released into a glass bulb by warming up the trap until the desired $CH_4$ pressure was obtained.

The following reaction sequence was used when the two-step reaction was carried out: (1) purified methane gas was introduced into the reactor with the clean crystal and the reaction then carried out at the desired reaction temperature for 5 min; (2) the crystal temperature was lowered as the methane was pumped simultaneously from the reactor; (3) hydrogen gas was admitted to the reactor and the second-step reaction was run. After the 10 min hydrogenation reaction, the product gas mixture was analyzed with gas chromatography (GC) utilizing a flame ionization detector.

HREELS data were collected in the second chamber following the first-step reaction. The spectra were acquired using an electron beam with a primary energy of $E_p \approx 2$–4 eV and at an incident angle of 60° from the surface normal. The other parameters used in obtaining the EELS spectra presented here were the following: spectral resolution (full width at half maximum of elastically reflected electron beam), 50–60 $cm^{-1}$; typical count rate in the elastic peak of the clean surface, 500000 Hz.

## 3. Results and discussion

### 3.1. SURFACE SPECTROSCOPIC IDENTIFICATION OF HYDROCARBON SPECIES FROM METHANE DECOMPOSITION

The decomposition of $CH_4$ on Ru(0001) and Ru(11$\bar{2}$0) surfaces was carried out

in the reactor of the HREELS UHV chamber. HREELS was used to identify various hydrocarbonaceous species on the Ru catalysts after the first-step reaction. Displayed in fig. 1 are HREELS spectra acquired following methane decomposition on Ru(0001) as a function of the first-step reaction temperature, $T_{CH_4}$. Exposing the surface to methane gives rise to several distinct loss features in the 200–4000 $cm^{-1}$ frequency range of the HREELS spectra. Two sets of loss features can be easily recognized from fig. 1. A dominant loss peak at 790 $cm^{-1}$ and a weak feature at 3000 $cm^{-1}$ are observed in the 400–700 K temperature range, while two weaker loss peaks at 1160 and 1395 $cm^{-1}$ are evident only at temperatures between 500 and 550 K in the HREELS spectra. These two sets of loss peaks apparently arise from two different surface intermediates. By analogy to the results obtained

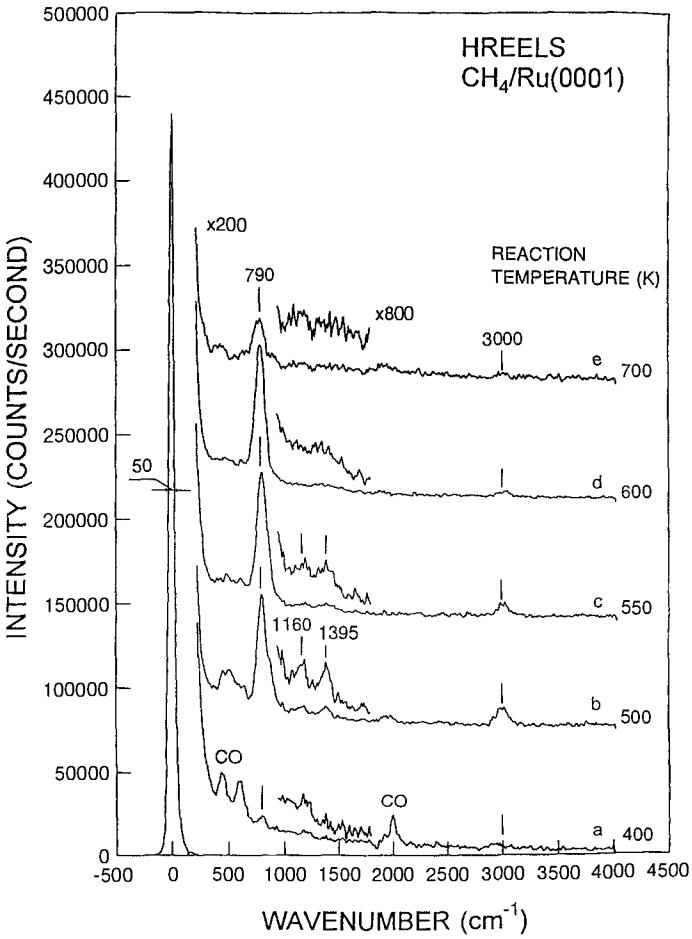


Fig. 1. HREELS spectra acquired following methane decomposition on Ru(0001) as a function of the reaction temperature, $T_{CH_4}$. The reaction was carried out with 5 Torr of methane for 120 s. The spectra were collected at $E_p \approx 4.1$ eV and at the specularly reflected beam direction.

from other HREELS studies and those of organometallic compounds, the two species are identified as the methylidyne (CH) and vinylidene ($CCH_2$) species, respectively [33]. The detailed assignment of the observed losses and identification of the corresponding hydrocarbon species are described elsewhere [33].

Two weak loss features at 475 and 2000 $cm^{-1}$, which arise from adsorbed CO, are noticeable at 400 K, as seen in spectrum a of fig. 1. Considering the high cross section of CO vibrational modes, the coverage of the CO impurities is estimated to be negligibly low. One also observes a weak feature at $\sim$ 600 $cm^{-1}$ which likely arises from a sub-surface oxygen species [33], as shown in spectrum a of fig. 1.

Fig. 2 shows HREELS spectra acquired of a Ru(11$\bar{2}$0) surface following reaction with methane as a function of the reaction temperature, $T_{CH_4}$. Similar to

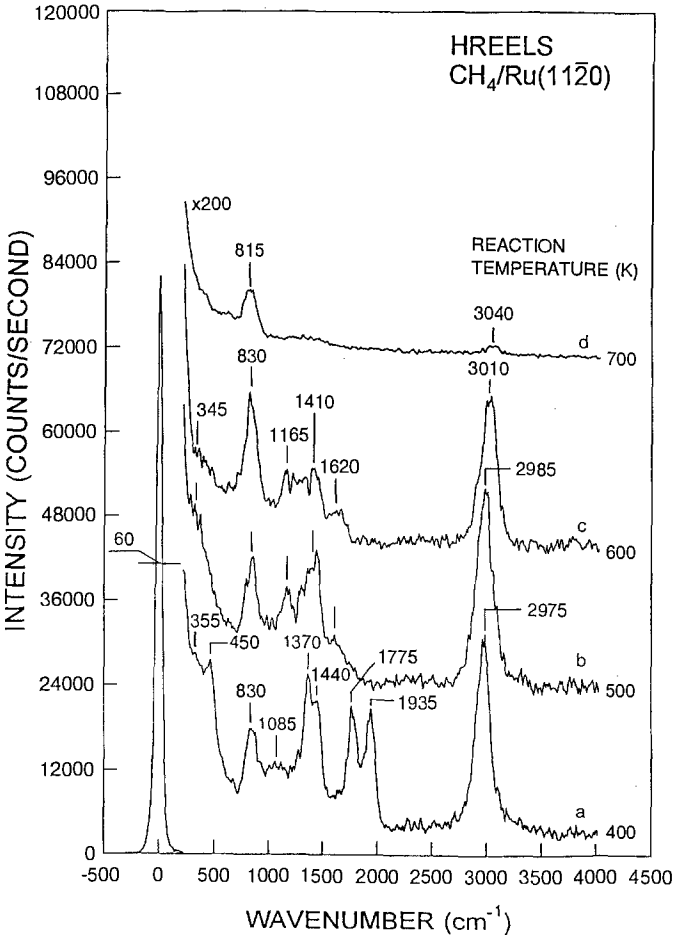


Fig. 2. HREELS spectra acquired following methane decomposition on Ru(11$\bar{2}$0) as a function of the reaction temperature, $T_{CH_4}$. The reaction was carried out with 5 Torr of methane for 120 s. The spectra were collected at $E_p \approx 2.2$ eV and at the specularly reflected beam direction.

decomposition of $CH_4$ on Ru(0001), two sets of loss features are easily recognizable at $T \geqslant 500$ K. These correspond to two different surface intermediates: methylidyne (CH) and vinylidene ($CCH_2$). Two loss peaks observed at 830 and 3010 $cm^{-1}$ arise from one type of surface species (methylidyne) and losses at $\sim$ 345, 1165, 1410, 1620 and 2985 $cm^{-1}$ are due to the other (vinylidene). The detailed assignment of these loss features and identification of the corresponding surface species are described elsewhere [33].

Besides the loss features arising from the methylidyne species, a new set of loss peaks is observed at $\sim$ 355, 1085, 1370, 1440 and 2975 $cm^{-1}$, as shown in spectrum a of fig. 2. These features apparently arise from a new surface species which differs from CH and $CCH_2$. Likewise, we identify this new species as an ethylidyne ($CCH_3$) species [33]. The additional losses at 450, 1775 and 1935 $cm^{-1}$ in spectrum a of fig. 2 are due to adsorbed CO.

Finally, it is noteworthy that there is a barely perceptible feature between 1100 and 1500 $cm^{-1}$ in spectra d and e of fig. 1, and also in spectrum d of fig. 2. This weak feature, which is observed only at temperatures exceeding 600 K, likely arises from the ring breathing mode of surface graphite [33].

In summary, the above HREELS studies reveal that three distinct forms of surface carbonaceous species, identified as methylidyne, vinylidene and graphitic carbonaceous species, exist on both the Ru(0001) and Ru(11$\bar{2}$0) surfaces following methane decomposition. A fourth species, ethylidyne, exists only on Ru(11$\bar{2}$0) surfaces at $T_1 \leqslant 400$ K. The methylidyne intermediate is observed in a wide temperature range between approximately 400 and 700 K. The vinylidene species is found to be less thermally stable than the methylidyne species and is present only at temperatures between 500 and 600 K. The graphitic carbon species is found at temperatures exceeding 600 K, and is associated with a very weak feature found between 1100 and 1500 $cm^{-1}$ in the specular HREELS spectra.

### 3.2. ELEVATED PRESSURE KINETIC STUDIES

Figs. 3a and 3b show yields of ethane and propane over Ru(0001) and Ru(11$\bar{2}$0) catalysts, respectively, as a function of the inverse first-step reaction temperature, $1/T_{CH_4}$. The yields presented here represent numbers of ethane and propane molecules produced from the two-step reaction, normalized to the surface density ($n = 1.58 \times 10^{15}$ $cm^{-2}$ for Ru(0001) and $n = 1.00 \times 10^{15}$ $cm^{-2}$ for Ru(11$\bar{2}$0)) of the Ru catalyst. The reaction conditions used here were: $P_{CH_4} = 5$ Torr, $t_{CH_4} = 5$ min; $P_{H_2} = 10$ Torr, $t_{H_2} = 10$ min, $T_{H_2} = 375$ K. Besides methane, ethane, propane and butane were detected in our experiments. The yield for every subsequent hydrocarbon addition decreases about tenfold, indicating a chain growth probability of 0.1. As shown in figs. 3a and 3b, the yields of ethane and propane first increase with an increase in $T_{CH_4}$ and decrease at temperatures exceeding 500 K. At $T_{CH_4} = 800$ K, the production of ethane and propane was negligible. There is no significant difference between the Ru(0001) and Ru(11$\bar{2}$0) cata-

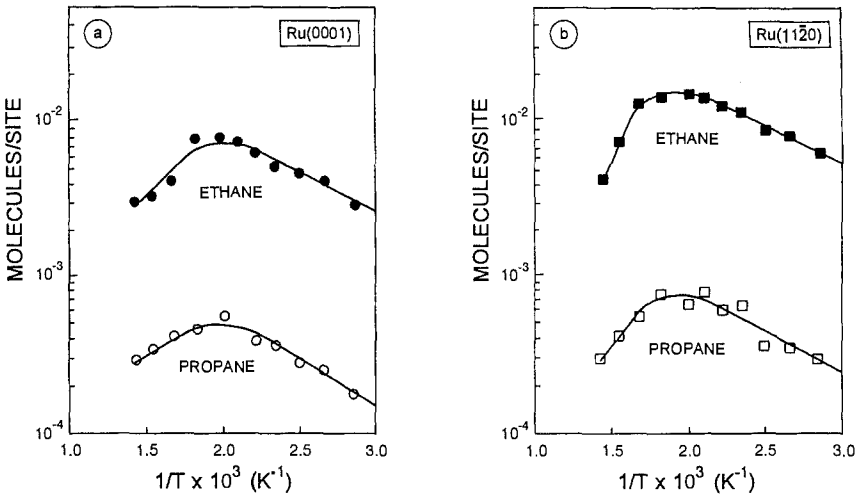


Fig. 3. Yields of ethane and propane plotted as a function of the inverse first-step reaction temperature, $1/T_{CH_4}$, over (a) Ru(0001) and (b) Ru(11$\bar{2}$0). The reaction conditions used were: $P_{CH_4} = 5$ Torr, $t_{CH_4} = 5$ min; $P_{H_2} = 10$ Torr, $t_{H_2} = 10$ min, $T_{H_2} = 375$ K.

lysts in the production of ethane and propane, although the yields of ethane and propane are slightly higher from Ru(11$\bar{2}$0) than from Ru(0001).

The carbon surface coverage following methane decomposition was obtained by measuring the peak-to-peak height ratio of the 273 eV Ru to 231 eV Ru Auger signals [30]. Since the detection of fractional monolayers of carbon on Ru is difficult because of the interference between the Ru (273 eV) and C (272 eV) transitions, the carbon coverages determined by this method contain relatively large error bars, particularly in the low coverage region. Figs. 4a and 4b show two plots of the Auger data acquired from Ru(0001) and Ru(11$\bar{2}$0) surfaces, respectively, before and after hydrogenation. It is seen that on both surfaces, the amount of deposited carbon increases monotonically with an increase in $T_{CH_4}$ and reaches the saturation or monolayer coverage at $T_{CH_4} = 800$ K. However, the temperature dependence of the carbon coverage appears to be different between Ru(0001) and Ru(11$\bar{2}$0) catalysts after hydrogenation. On a Ru(0001) surface, the amount of remaining carbon residues increases linearly with $T_{CH_4}$, whereas the carbon coverage on a Ru(11$\bar{2}$0) surface remains essentially constant up to 500 K and then increases sharply at temperatures exceeding 500 K.

Displayed in figs. 5a and 5b are the differences in carbon coverage between the first- and the second-step reaction. The differences in the coverages represent the amount of the carbon removed, namely the active carbon. On the Ru(0001) surface, the coverage of the active carbon decreases with an increase in $T_{CH_4}$, whereas on Ru(11$\bar{2}$0), a maximum in the active carbon coverage is observed at 500 K (see fig. 5).

The above results show that on the Ru(11$\bar{2}$0) surface, the yields of ethane and

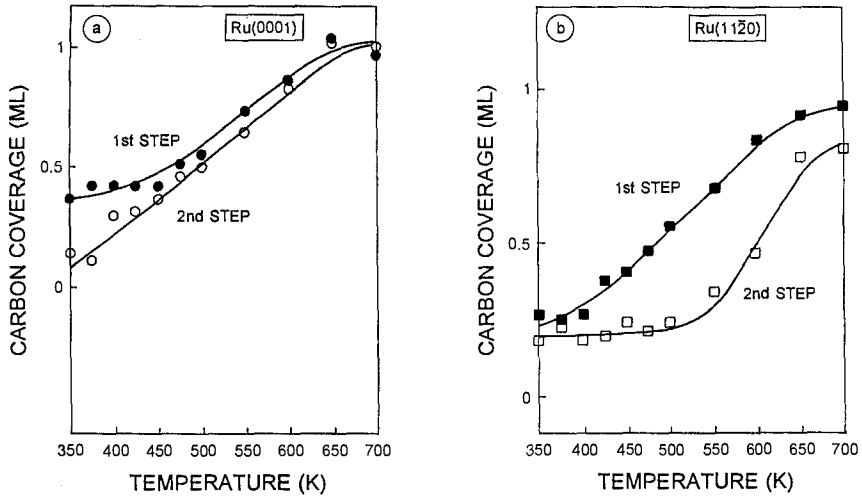


Fig. 4. Carbon coverage after the first- and second-step reaction as a function of $T_{CH_4}$: (a) Ru(0001); (b) Ru(11$\bar{2}$0). The carbon coverage was determined using the peak-to-peak height ratio of the 273 eV Ru to 231 eV Ru Auger signal. The reaction conditions used were the same as those of fig. 3.

propane parallel the active carbon coverage. A comparison with the HREELS results reveals immediately that the active carbon species is derived from vinylidene and methylidyne intermediates. At $T_{CH_4} \leqslant 400$ K, the ethylidyne species may also be the active form of carbon. One notices that the respective contribution of

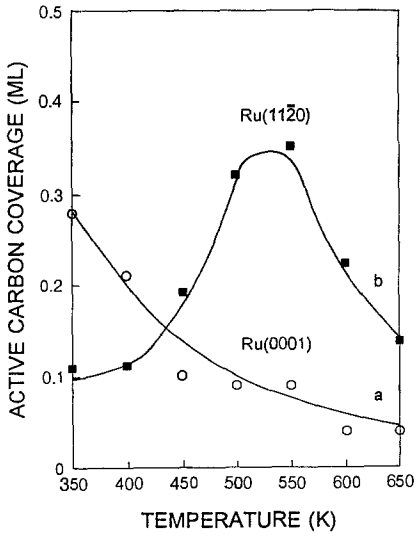


Fig. 5. Difference in carbon coverage between the first- and second-step reaction as a function of $T_{CH_4}$: (a) Ru(0001); (b) Ru(11$\bar{2}$0). The difference in the coverages represents the amount of the carbon removed, namely the active carbon.

the methylidyne and vinylidene intermediates to the ethane and propane production is difficult to evaluate based on the relative mode intensities of these species in the HREELS spectra. However, the vinylidene species is likely to be the key intermediate to ethane for the following reasons. First, on both the Ru(11$\bar{2}$0) and Ru(0001) surfaces, the maximum in ethane and propane production coincides with the maximum HREELS intensities of the vinylidene intermediates, as shown in figs. 1 and 2. Second, hydrogenation of the vinylidene intermediates directly to ethane should be easier than polymerization and hydrogenation of the methylidyne species to ethane. However, one may not rule out that a portion of the methylidyne species may polymerize to form vinylidene intermediates and then hydrogenate to form ethane. Clearly, further studies including quantifying the respective contribution of the observed hydrocarbon species to the ethane production are needed to verify the above reaction mechanisms.

On the Ru(0001) surface, the maximum in ethane and propane production does not appear to coincide with the maximum coverage of active carbon. The coverage of the active carbon decreases with an increase in $T_{CH_4}$, whereas the yields of ethane and propane maximize at $T_{CH_4} \approx 500$ K. However, the HREELS spectra of fig. 1 indicate that the loss features arising from the methylidyne and vinylidene intermediates are more intense in the 500–600 K temperature range than those observed at $T_{CH_4} < 500$ K or $T_{CH_4} > 600$ K.

Plotted in figs. 6a and 6b are the selectivities for ethane and propane formation on Ru(0001) and Ru(11$\bar{2}$0) surfaces, respectively. Under the optimum reaction conditions, hydrocarbon products consist of $\sim$ 16% ethane and $\sim$ 2% propane. There is no significant difference in the optimum selectivity on either surface. How-

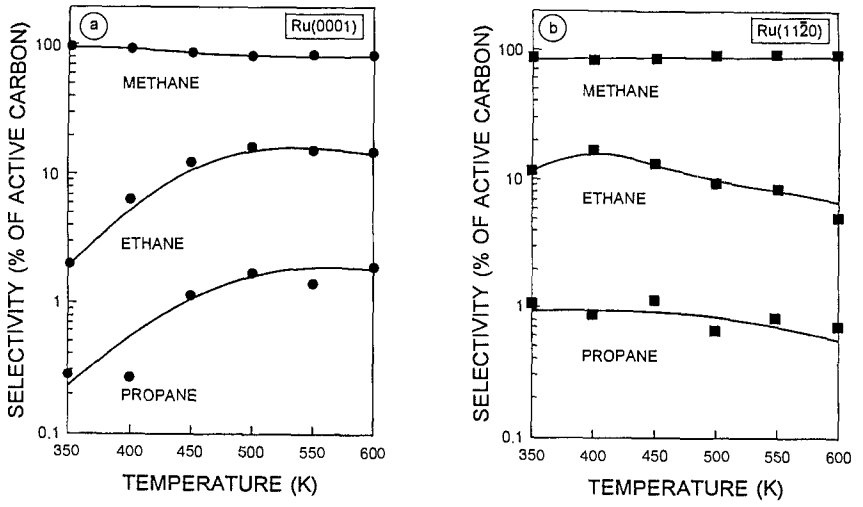


Fig. 6. Selectivity for the formation of methane, ethane and propane as a function of $T_{CH_4}$: (a) Ru(0001); (b) Ru(11$\bar{2}$0).

ever, the temperature dependence of the selectivity between the two surfaces appears different. On the (0001) face of ruthenium, the selectivities for ethane and propane formation increase with an increase in $T_{CH_4}$ and reach a plateau for $T_{CH_4}$ exceeding 500 K. On Ru(11$\bar{2}$0) surfaces, the selectivity in ethane formation maximizes at 400 K and decreases gradually to 5% at 600 K.

Figs. 7a and 7b show yields of ethane and propane from Ru(0001) and Ru(11$\bar{2}$0), respectively, versus the inverse hydrogenation temperatures, $1/T_{H_2}$. The reaction conditions used here were: $P_{CH_4} = 1$ Torr, $t_{CH_4} = 5$ min, $T_{CH_4} = 425$ K; $P_{H_2} = 10$ Torr, $t_{H_2} = 10$ min. On Ru(0001), the yields of ethane and propane maximize at $T_{H_2} = 400$ K, whereas no maximum yield was observed on Ru(11$\bar{2}$0) in the 300–500 K temperature range. It was found that the carbon coverages after the second-step reaction were independent of the hydrogenation temperature, $T_{H_2}$.

The yields of ethane and propane obtained from Ru(0001) and Ru(11$\bar{2}$0) surfaces as a function of time, $t_{CH_4}$, are plotted in figs. 8a and 8b, respectively. The reactions were carried out at three different temperatures of $T_{CH_4} = 425$, 500 and 600 K. The other reaction parameters used were: $P_{CH_4} = 5$ Torr; $P_{H_2} = 10$ Torr, $t_{H_2} = 10$ min, $T_{H_2} = 375$ K. The following procedure was used when the data points in figs. 8a and 8b were collected: (1) each data point of figs. 8a and 8b represents one reaction cycle consisting of methane decomposition and hydrogenation; (2) there is no cleaning between each cycle. It can be seen from figs. 8a and 8b that at $T_{CH_4} = 425$ K, the yields of ethane and propane do not change with the number of cycles. The yields of ethane and propane, however, decrease at $T_{CH_4} = 500$ and 600 K with an increase in the number of cycles. These results clearly indicate the formation of the passive form of carbon at these high temperatures.

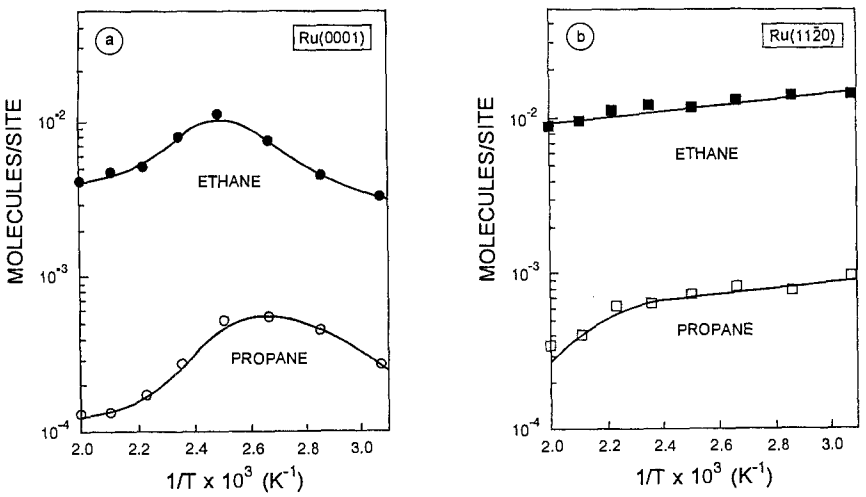


Fig. 7. Yields of ethane and propane plotted as a function of the inverse second-step reaction temperature, $1/T_{H_2}$: (a) Ru(0001), (b) Ru(11$\bar{2}$0). The reaction conditions used were: $P_{CH_4} = 1$ Torr, $t_{CH_4} = 5$ min, $T_{CH_4} = 425$ K; $P_{H_2} = 10$ Torr, $t_{H_2} = 10$ min.

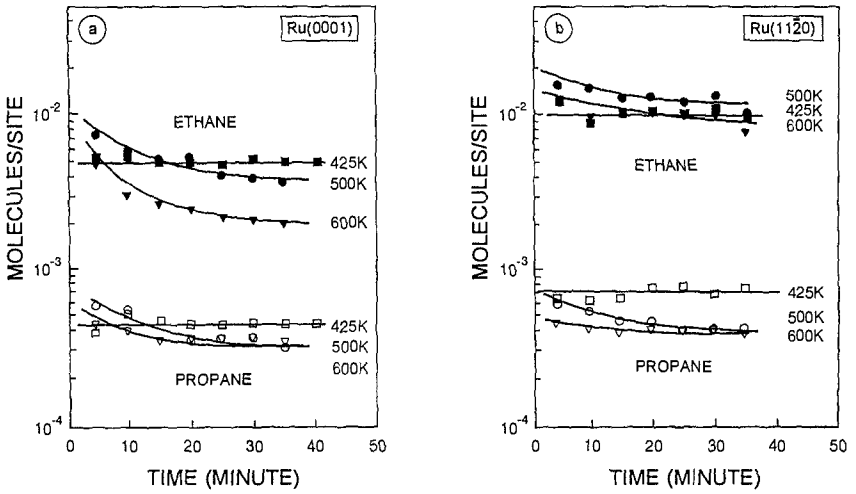


Fig. 8. Yields of ethane and propane obtained as a function of the first-step reaction time: (a) Ru(0001), (b) Ru(11$\bar{2}$0). The reactions were carried out at three different temperatures of $T_{CH_4}$ = 425, 500 and 600 K. The other parameters used were: $P_{CH_4}$ = 5 Torr, $P_{H_2}$ = 10 Torr, $t_{H_2}$ = 10 min, $T_{H_2}$ = 375 K.

## 4. Summary

The conversion of methane to ethane and propane on Ru(0001) and Ru(11$\bar{2}$0) catalysts has been investigated using combined elevated-pressure kinetic measurements/surface science studies. The yields of ethane and propane have been measured using gas chromatography as a function of the first- and second-step reaction temperature. It was found that the maximum yield in ethane/propane production occurs for a methane decomposition temperature at $T_{CH_4}$ = 500 K on both the surfaces. The influence of the hydrogenation temperature on the production of ethane and propane was also examined. On Ru(0001), the yields of ethane and propane maximize at $T_{H_2}$ = 400 K, whereas no maximum yield was observed on Ru(11$\bar{2}$0) in the 300–500 K temperature range. Under optimum reaction conditions, hydrocarbon products consist of 16% ethane and 2% propane.

High-resolution electron energy-loss spectroscopy (HREELS) has been used to identify various forms of hydrocarbon intermediates following methane decomposition. Three distinct forms of surface carbon species, identified as methylidyne, vinylidene and graphitic carbonaceous species, exist on both the Ru(0001) and Ru(11$\bar{2}$0) surfaces following methane decomposition. The fourth species, ethylidyne, exists only on Ru(11$\bar{2}$0) surfaces at $T_{CH_4} \leqslant 400$ K. Our combined elevated pressure measurements/HREELS studies show that the vinylidene species is likely to be the key intermediate to ethane.

## Acknowledgement

We acknowledge the support of this work by the Gas Research Institute and Amoco Corporation.

## References

[1] J.R. Rostrup-Nielsen, *Catalysis: Science and Technology*, eds. J.R. Anderson and M. Boudart (Springer, Berlin, 1984).
[2] M.A. Vannice, Catal. Rev.-Sci. Eng. 14 (1976) 153.
[3] H. Pichter, Advan. Catal. 4 (1952) 271.
[4] T. Ito and J.H. Lunsford, Nature 314 (1985) 721.
[5] D.J. Driscoll, W. Martir, J.-X. Wang and J.H. Lunsford, J. Am. Chem. Soc. 107 (1985) 58.
[6] T. Ito, J.-X. Wang, C.-H. Lin and J.H. Lunsford, J. Am. Chem. Soc. 107 (1985) 5062.
[7] T. Koerts and R.A. van Santen, J. Chem. Soc. Chem. Commun. (1991) 1281.
[8] K. Coulter and D.W. Goodman, Catal. Lett. 16 (1992) 191.
[9] J.H. Lunsford, Catal. Today 6 (1990) 235.
[10] T. Koerts and R.A. van Santen, J. Chem. Soc. Chem. Commun. (1991) 1281.
[11] T. Koerts, M.J.A.G. Deelen and R.A. van Santen, J. Catal. 138 (1992) 101.
[12] T. Koerts and R.A. van Santen, J. Mol. Catal. 70 (1991) 119.
[13] G.C. Bond, *Catalysis by Metals* (Academic Press, New York, 1962).
[14] M.B. Lee and Q.Y. Yang, J. Chem. Phys. 85 (1986) 1693.
[15] J.D. Beckerle, Q.Y. Yang, A.D. Johnson and S.T. Ceyer, J. Chem. Phys. 86 (1987) 7236.
[16] M.T. Travares, C.A. Bernardo, J. Alstrup and J.R. Rostrup-Nielsen, J. Catal. 100 (1986) 545.
[17] S.G. Brass and G. Ehrlich, Surf. Sci. 191 (1987) L819.
[18] S.G. Brass and G. Ehrlich, Surf. Sci. 187 (1987) 21.
[19] E.G.M. Kuijpers, J.W. Janson, A.J. VanDillen and J.W. Geuss, J. Catal. 72 (1981) 75.
[20] Y.K. Sun and W.H. Weinberg, J. Vac. Sci. Technol. A 8 (1990) 2445.
[21] A.G. Sault and D.W. Goodman, Advan. Chem. Phys. 76 (1989) 153.
[22] M.B. Lee, Q.Y. Yang and S.T. Ceyer, J. Chem. Phys. 87 (1987) 2724.
[23] A.D. Johnson, J. Maynard, S.P. Daley, Q.Y. Yang and S.T. Ceyer, Phys. Rev. Lett. 67 (1991) 927.
[24] J.D. Beckerle, A.D. Johnson, Q.Y. Yang and S.T. Ceyer, J. Chem. Phys. 91 (1989) 5756.
[25] J.D. Beckerle, A.D. Johnson and S.T. Ceyer, J. Am. Chem. Soc. 62 (1989) 685.
[26] T.M. Duncan, P. Winslow and A.T. Bell, J. Catal. 93 (1985) 1.
[27] P. Winslow and A.T. Bell, J. Catal. 86 (1984) 158.
[28] T.M. Duncan, P. Winslow and A.T. Bell, J. Catal. 95 (1985) 226.
[29] M.-C. Wu, C.A. Estrada, J.S. Corneille and D.W. Goodman, J. Chem. Phys. 96 (1992) 3892.
[30] D.W. Goodman and J.M. White, Surf. Sci. 90 (1979) 201.
[31] G. Lauth, E. Schwartz and K. Christman, J. Chem. Phys. 91 (1989) 3729.
[32] G. Lauth, T. Solomun, W. Hirschwald and K. Christman, Surf. Sci. 210 (1989) 201.
[33] M.-C. Wu and D.W. Goodman, J. Am. Chem. Soc., in press.